Chapter 15

Alternative BSM Signatures

15.1 Technicolour

15.1.1 The $\rho_{TC} \rightarrow W + Z$ channel

Technicolour (TC) provides an alternative to the elementary Higgs mechanism of the Standard Model. It introduces a new strong interaction [745] providing a dynamical nature to Electroweak Symmetry Breaking. Technicolour is a QCD-like force, acting on technifermions at an energy scale $\Lambda_{TC} \sim \nu_{weak}$ = 246 GeV. A number N_D of technifermion doublet condensates yield the pseudo-Goldstone bosons π_{TC}, together with a wide spectroscopy of excited technimesons. The present simulation is performed using the phenomenology of the lowest-lying technihadrons, commonly referenced as the "Technicolour Straw Man" model (TCSM) [735]. The colour-singlet sector includes the spin-zero π_{TC} and the spin-one technimesons ρ_{TC} and ω_{TC}. The decay cross-section of the ρ_{TC} is expressed as an admixture of π_{TC} and the Standard Model Z and W bosons:

$$\rho_{TC} \rightarrow \cos^2\chi < \pi_{TC}\,\pi_{TC} > + \cos\chi \sin\chi < \pi_{TC}\,V_L > + \sin^2\chi < V_L V_L > \qquad (15.1)$$

where V_L is the longitudinal mode of the $V = Z, W$ and $\sin\chi \simeq 1/\sqrt{N_D} \sim 1/3$. The branching fraction BR($\rho_{TC} \rightarrow W + Z$) is competing with the two first terms in Eq. 15.1, hence changing with M(π_{TC}).

The decay channel $\rho_{TC} \rightarrow W + Z$ is the subject of this analysis [746] as it has the advantage of a very clean final state, namely $3\ell + \nu$. The background contributions arise mainly from Standard Model processes involving weak boson production and decays. Other Technicolour decay modes that include jets such as $\rho_{TC} \rightarrow \pi_{TC} + W$, have higher branching fractions but are much harder to disentangle from the Standard Model background processes.

15.1.1.1 Event selection

All signal and backgrounds samples used in this analysis are generated with PYTHIA 6.2 [24] with the requirement of at least 3 prompt leptons in the CMS fiducial region. The $Zb\bar{b}$ background is generated using COMPHEP [354] interfaced to PYTHIA. Contributions from processes of type $Z \rightarrow 2\ell$ plus an additional fake lepton from a jet have been taken into account in the systematic uncertainties, see Sect. 15.1.1.2. A set of 14 different ρ_{TC} samples are generated within the $[\,\mathrm{M}(\rho_{TC}),\, \mathrm{M}(\pi_{TC})\,]$ phase space.
Nominal CMS Level-1 and High-Level Trigger requirements are applied [75]. The CMS fast simulation [11] is used for detector simulation and event reconstruction. The main reconstructed objects and their efficiencies have been validated against the detailed GEANT-based CMS detector simulation [8, 10].

The analysis is designed to reduce the main Standard Model background contributions WZ, ZZ, $Zb\bar{b}$ and $t\bar{t}$, while retaining high signal efficiency. It is summarised as follows:

(i) Lepton selection: 3 high-$p_{\rm T}$ and isolated electrons or muons.
(ii) Lepton trigger: single- or two-electron or muon mode (Level-1 and HLT)
(iii) Z: same-flavour and opposite-charge ℓ-pair closest to M(Z), with $p_{\rm T}$ ($\ell_{1,2}$) > (30,10) GeV/c
(iv) W: solution to 3rd lepton with $p_{\rm T} > 10$ GeV/c + Missing $E_{\rm T}$ + M(W) constraint
(v) $|\,{\rm M}(\ell^+\ell^-) - {\rm M}(Z)\,| \leq 3\sigma_{{\rm M}_Z} \cong 7.8$ GeV/c^2
(vi) $p_{\rm T}$ (Z) and $p_{\rm T}$ (W) > 30 GeV/c. For benchmark points with M(ρ_{TC}) = 200 GeV/c^2, the minimum $p_{\rm T}$ (Z) and $p_{\rm T}$ (W) threshold is 10 GeV/c.
(vii) $|\Delta[\eta(Z) - \eta(W)]| \leq 1.2$

The Z and W are reconstructed with a purity of ∼99%, using the 3 highest-$p_{\rm T}$ leptons in the event, and the Missing Transverse Energy (MET), obtained as the vector sum of the jets and leptons in the event. The M(W) constraint yields a 2 fold ambiguity in the $p_{\rm Z}$ component of the reconstructed neutrino: it is found that the most efficient choice for the ρ_{TC} signal is the minimum $p_{\rm Z}$ solution. The kinematic cuts are illustrated in Fig. 15.1. The main $t\bar{t}$ reduction is obtained via the Z-mass window requirement (v). The irreducible background $WZ \to 3\ell + \nu$ is most efficiently separated from the signal via the $\eta(Z) - \eta(W)$ correlation requirement (vii).

The $p_{\rm T}$ cut on Z and W further improves the signal to background ratio, however it is kept modest in order to preserve the exponential background hypothesis of the $3\ell + \nu$ invariant mass spectrum, used to compute the signal sensitivity. The $\rho_{TC}(300, 300)$ signal and background yields are shown in Fig. 15.1(d) and the corresponding reconstruction efficiencies are listed in Table 15.1.

Table 15.1: σ x BR ($\ell =$ e or μ), 3-lepton pre-selection efficiency, total efficiency and final yield within 3σ of the signal region (Nev), for $\mathcal{L} = 5$ fb^{-1}. $\rho_{TC}(300, 300)$ and the main background contributions are shown. The simulation is repeated for all ρ_{TC} benchmark points.

Sample	σxBR(pb)	ϵ(3-lept)	ϵ(Reco) (%)	Nev(5 fb^{-1})
$\rho_{TC} \to W + Z \to 3\ell + \nu$	0.13	0.635	25.88 +- 0.40	103
$WZ \to 3\ell + \nu$	0.39	0.471	9.91 +- 0.11	27
$ZZ \to 4\ell$	0.07	0.719	15.80 +- 0.14	10
$Zb\bar{b} \to 2\ell + X$	332	0.046	0.23 +- 0.01	12
$t\bar{t}$	489.72	0.065	0.019 +- 0.001	8

15.1.1.2 Signal sensitivity and systematic uncertainties

The sensitivity of each ρ_{TC} benchmark point is computed by taking into account realistic statistical fluctuations for a given integrated luminosity. The sensitivity estimator is defined as the likelihood-ratio S_L, defined in Appendix A.1, The signal probability density function (p.d.f.) is assumed Gaussian (dominated by detector resolution) and the background p.d.f. is Exponential in all ρ_{TC} fit regions. The output of the fitting procedure is shown in the contour plot over the [M(ρ_{TC}), M(π_{TC})] phase space in Fig. 15.2(a), for various integrated luminosities. A signal sensitivity above 5 is expected for $\mathcal{L} = 3$ fb^{-1} (before including systematic uncertainties).

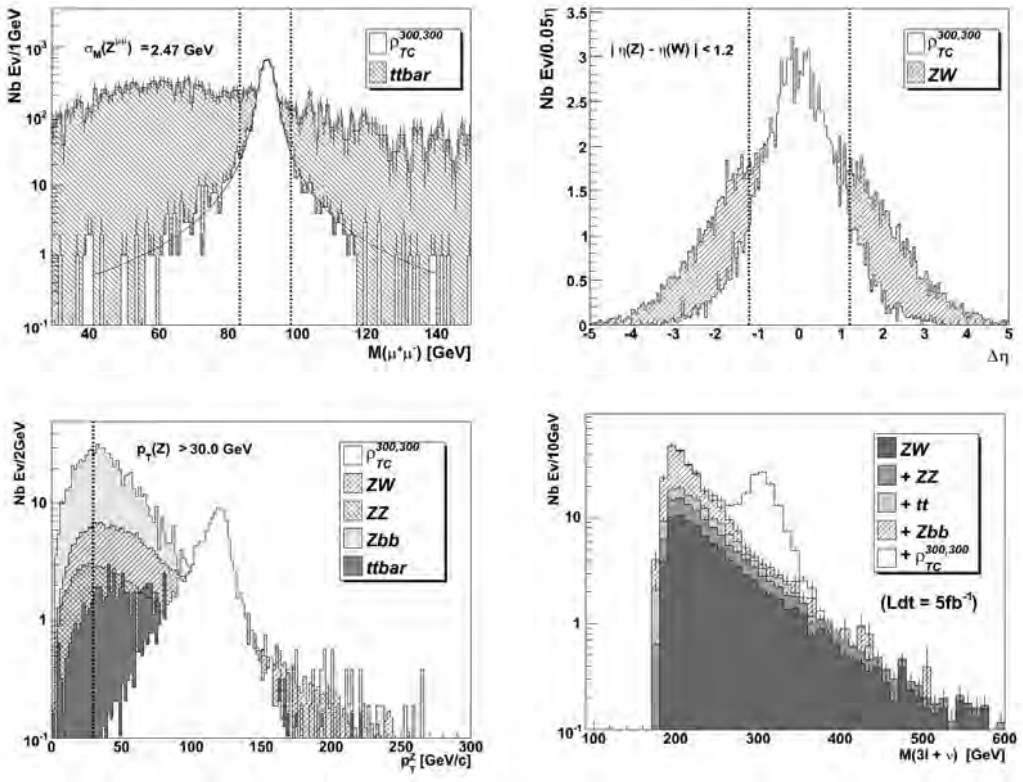

Figure 15.1: (a) $\mathrm{M}(\mu^+\mu^-)$ for $\rho_{TC}(300,300)$ and $t\bar{t}$; (b) $\Delta[\eta(\mathrm{Z})-\eta(\mathrm{W})]$ for $\rho_{TC}(300,300)$ and WZ; (c) p_{T} (Z) for $\rho_{TC}(300,300)$ and all backgrounds (p_{T} (W) is similar); (d) Reconstructed $\mathrm{M}(3\ell+\nu)$ for $\rho_{TC}(300,300)$ and all backgrounds. The vertical lines indicate the applied requirements.

The ρ_{TC} sensitivity has been simulated for the early CMS data taking phase. Expected detector related systematic uncertainties for $\mathcal{L} = 1\,\mathrm{fb}^{-1}$ are taken into account. While no substantial contribution is found from the tracker and muon system misalignment or the calorimeter miscalibration, the accuracy at which the lepton efficiency will be determined from data affects the result: a 2% uncertainty is considered. Moreover, the lepton fake rate has been simulated on $Zb\bar{b}$ and extrapolated to any $Z+jet(s)$ type background, *, in order to take into account additional contaminations from pion/kaon decays or from wrongly identified lepton candidates. A production cross-section of 1047pb per lepton flavour is assumed for $Z + n\text{-}jets$, $n \geq 0$. A single lepton fake rate of O(10^{-3}) is obtained using the fast simulation [11], affecting the ρ_{TC} sensitivity as shown below. Finally, a 7.5% uncertainty on the missing transverse energy measurement is considered. The above uncertainties result in the following relative ρ_{TC} sensitivity drop:

$$\Delta^{\mathrm{tot}}_{\mathrm{SYS}} = \sqrt{(\Delta^{\mathrm{Eff}}_{\mathrm{SYS}})^2 + (\Delta^{\mathrm{Fake}}_{\mathrm{SYS}})^2 + (\Delta^{\mathrm{MET}}_{\mathrm{SYS}})^2} = \sqrt{(2.7\%)^2 + (8.5\%)^2 + (6.6\%)^2} = 11\% \quad (15.2)$$

Introducing K-factors from Next-to-Leading-Order (NLO) expectations for the signal (a K-factor 1.35 is assumed in similarity with the Drell-Yan process) and background leads to a relative signal sensitivity increase of 6%; however the latter estimate has not been included

*A production cross-section of 1047pb per lepton flavour is assumed for $Z + n\text{-}jets$, $n \geq 0$.

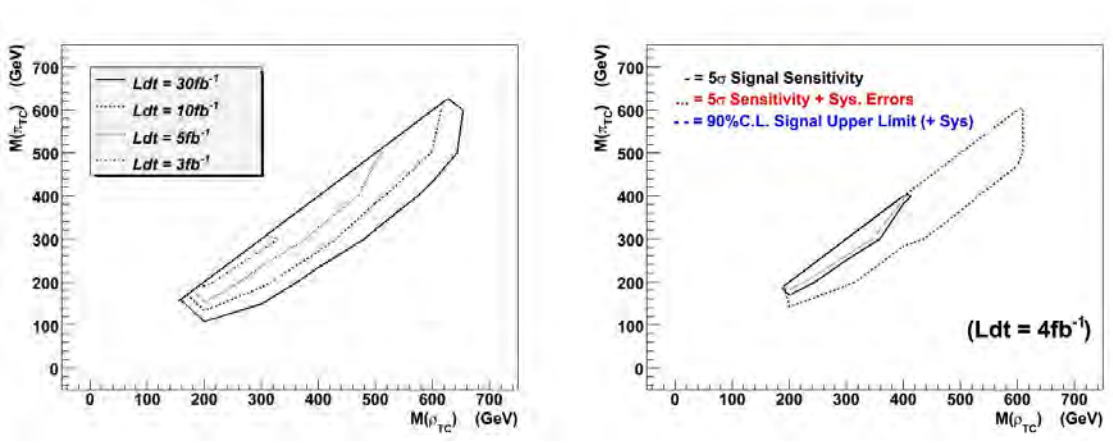

Figure 15.2: (left) Signal 5σ Sensitivity curves for various integrated luminosities; (right) sensitivity for $\mathcal{L} = 4\,\text{fb}^{-1}$: the dotted (resp. dashed) curve shows the sensitivity (resp. the 90% C.L. signal upper limit) after including systematic uncertainties.

in the final result.

In summary, the technicolour signature $\rho_{TC} \to W + Z$ in the context of the Straw Man model is studied. The 5 sigma discovery reach is obtained for an integrated luminosity $\mathcal{L} \simeq 4\,\text{fb}^{-1}$.

15.2 Search for contact interactions with dimuons

Contact interactions offer a general framework for describing a new interaction with typical energy scale $\Lambda \gg \sqrt{s}$. The presence of operators with canonical dimension $N > 4$ in the Lagrangian gives rise to effects $\sim 1/\Lambda^{N-4}$. Such interactions can occur for instance, if the SM particles are composite, or when new heavy particles are exchanged.

Table 15.2: Contact interaction models.

Model	LL	RR	LR	RL	VV	AA	LL+RR	LR+RL
	Non-parity conserving				Parity conserving			
η_{LL}	±1	0	0	0	±1	±1	±1	0
η_{RR}	0	±1	0	0	±1	±1	±1	0
η_{LR}	0	0	±1	0	±1	∓1	0	±1
η_{RL}	0	0	0	±1	±1	∓1	0	±1

In the following we will consider lepton-pair production. The lowest order flavour-diagonal and helicity-conserving operators have dimension six [122].

The differential cross section takes the form

$$\frac{d\sigma}{d\Omega} = SM(s,t) + \varepsilon \cdot C_{Int}(s,t) + \varepsilon^2 \cdot C_{NewPh}(s,t) \tag{15.3}$$

where the first term is the Standard Model contribution, the second comes from interference between the SM and the contact interaction, and the third is the pure contact interaction effect. The Mandelstam variables are denoted as s, t and u.

Usually the coupling is fixed, and the structure of the interaction is parameterised by coefficients for the helicity amplitudes:

g	coupling (by convention $\frac{g^2}{4\pi} = 1$)
$\lvert\eta_{ij}\rvert \leq 1$	helicity amplitudes ($i, j = \mathrm{L}, \mathrm{R}$)
ε	$\frac{g^2}{4\pi}\frac{sign(\eta)}{\Lambda^2}$ for $f\bar{f}$

Some often investigated models are summarised in Table 15.2. The models in the second half of the table are parity conserving, and hence not constrained by the very precise measurements of atomic parity violation at low energies. The results presented in this contribution cover the LL model, which has the highest sensitivity at LHC energies from the models in the first half of the table. More details can be found in [348].

15.2.1 Analysis

The topology under study is high-mass muon pairs with opposite sign. More details on the analysis are found in [348]. The Global Muon Reconstructor (GMR, described in Vol.1, Section 9.1.2) output is used. The dimuon events are triggered by the single and dimuon triggers. We have processed events, generated to cover the whole region of interest up to dimuon masses of 6 TeV/c^2, through full simulation with OSCAR and reconstruction with ORCA. The dimuon mass resolution is parameterised in two ways:

- as mass dependent one standard deviation (RMS)
- by fitting the mass resolution with a sum of two Gaussians to account for the long tail of less well reconstructed masses.

The results are remarkably stable as a function of the dimuon mass: the second Gaussian contributes around 14% and has a standard deviation 3.3 times bigger than the first Gaussian.

Our strategy is to generate events with PYTHIA and apply parametrisations of the dimuon mass efficiency and resolution obtained from full simulation. We have verified our approach by comparing the resulting mass spectra with the ones obtained with OSCAR/ORCA or FAMOS for Drell-Yan and selected contact interactions samples, observing good agreement in all cases.

Two mass regions: 500–1000 GeV and 1000–6000 GeV are considered. The total cross section and the forward-backward asymmetry as function of the dimuon mass are studied. Our analysis shows that the sensitivity to contact interactions comes almost exclusively from the cross section measurements for the LL model.

In order to reduce the systematic uncertainties both on the experimental and theory sides a "double ratio" method is developed. The number of observed events for a given bin in invariant mass is

$$N_{obs} = L \cdot \sigma \cdot \varepsilon \tag{15.4}$$

where L is the luminosity, σ the differential cross section for the given mass bin, and ε the experimental efficiency. We select a zeroth "normalisation" bin for invariant masses between 250–500 GeV/c^2, both well above the Z pole and in an area well covered by the Tevatron, and define the experimental ratios

$$R_i^{DATA} = \frac{N_i^D}{N_0^D} = \frac{\sigma_i^D \cdot \varepsilon_i^D}{\sigma_0^D \cdot \varepsilon_0^D}. \tag{15.5}$$

Here the cross sections and efficiencies are the ones for the real LHC data. The index i runs for all measured bins with masses above 500 GeV/c^2. The luminosity cancels in the ratio. The choice of this mass bin is not random. If we compare the flavour composition of partons initiating the hard interaction (Table 15.3), at the Z peak 32.1% are heavier flavours (not u or d quarks), with their own parton density functions (PDF) uncertainties. At 250–500 GeV/c^2 the u and d quarks are "initiators" already in 85.6% of the cases, increasing to 96.3% above 1 TeV/c^2 etc. Moreover, at the Z peak d quarks are most abundant, while at higher masses u quarks dominate, asymptotically approaching a ratio 4:1. It is clear that our choice of normalisation bin gives flavour composition much closer to the most interesting high mass events, compared to a normalisation using Z pole events. The PDF uncertainty on cross sections is estimated using LHAPDF [94, 350]. It is interesting to note that this uncertainty reaches a minimum for masses 250–600 GeV/c^2, corresponding to medium values of the parton momentum fractions X, reinforcing our choice of normalisation bin.

Table 15.3: Flavour composition of partons initiating the hard Drell-Yan interaction.The PDF uncertainty on the cross sections (positive and negative asymmetric errors) is estimated using LHAPDF.

Mass [GeV/c^2]	d	u	s	c	b	PDF +	PDF -
			[%]			[%]	
Z peak	35.9	32.1	17.2	9.77	5.10	+4.7	-5.7
250-500	24.3	61.3	6.22	6.64	1.54	+3.4	-4.2
500-600	22.8	68.4	4.03	3.95	0.89	+3.5	-4.1
1000+	21.7	74.6	1.86	1.48	0.33	+5.0	-5.8
2000+	19.9	78.4	0.91	0.63	0.14	+9.0	-7.7

We define similar ratios for the Monte Carlo (theory) predictions. The *absolute* values of the cross sections and efficiencies are not important for the ratios, what matters is *the shape* of these quantities as function of invariant mass. For example, the absolute value of K-factors, a way to compensate for missing higher order N(N)LO terms and enable the comparison of leading order Monte Carlo predictions to data (similarly for the electroweak radiative corrections) disappears from the ratios and only the *shape* of the K-function as depending on invariant mass remains - a much smaller effect. And part of the uncertainties introduced due to our limited knowledge of PDFs cancels in the ratio, leaving smaller residual uncertainties due to the change of phase space for changing masses.

Now let us define the double ratios

$$DR_i = \frac{R_i^{DATA}}{R_i^{MC}}. \tag{15.6}$$

This method is inspired by a study of Drell-Yan events and extraction of proton and pion PDFs at lower masses [747], as well as by the SuperKamiokande double ratio method for measuring atmospheric neutrino oscillations [748]. If our theory understanding and detector modelling are both perfect, we expect $DR_i \equiv 1$. The experimental or Monte Carlo errors introduced in the ratios from the uncertainties in the zeroth bin are negligible, as due to the steeply falling Drell-Yan spectrum this bin has much more data compared to the high mass bins.

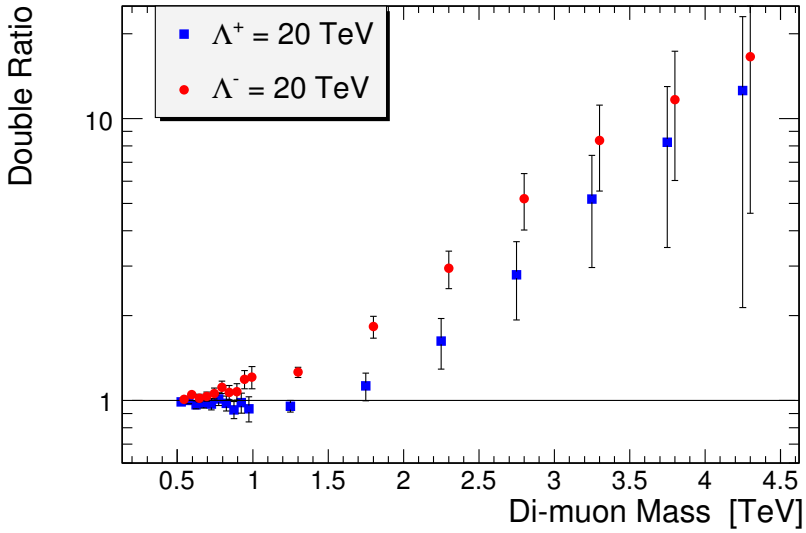

Figure 15.3: Double ratios for contact interactions in the dimuon channel, LL model, scale $\Lambda = 20\,\text{TeV/c}^2$, positive and negative interference, and luminosity $100\,\text{fb}^{-1}$. The errors shown are statistical.

An example of double ratios for positive and negative interference is shown in Figure 15.3. As can be seen, for scale $\Lambda = 20\,\text{TeV/c}^2$ the expected effects are quite sizable (note the log scale), with the sensitivity for negative interference starting around dimuon masses of $750\,\text{GeV/c}^2$, while for positive interference masses above $2\,\text{TeV/c}^2$ are required.

The experimental systematic effects in the cross section measurement are estimated to be 2% from the total muon efficiency and no more than 1.4% from momentum resolution. The former can be controlled quite well with the huge sample of Z events decaying to dimuons, and the effects for TeV muons are taken into account on top of this. The latter is important at high mass as smearing from lower masses from the steeply falling Drell-Yan spectrum can contaminate the high mass measurements, especially if the tails of the momentum resolution are not under control. It is estimated by varying the two parametrisations of the mass resolution by $\pm 40\%$, giving consistent results. The main source of systematic uncertainties on the momentum resolution comes from the alignment of the muon chambers and the central tracker, both at start-up and at high luminosity.

The systematic uncertainties from our limited knowledge of PDFs is estimated using the CTEQ6M PDF set from LHAPDF. From Table 15.4 our estimate of the PDF uncertainty on the cross section ratio is $^{+5.2}_{-4.8}$% above 1 TeV or $^{+10.7}_{-7.8}$% above 2 TeV.

The genuine electro-weak radiative corrections change by $\sim 10\%$ in the relevant mass range [157, 349]. The K-function changes faster below 250-300 GeV. From our normalisation bin to the highest masses first estimates show a change below 8% on the cross section [†]. Taking conservatively half of these changes with mass as an upper limit on the systematic uncertainty we arrive at 5% and 4% respectively.

Combining all effects in quadrature, we arrive conservatively at systematic uncertainties below 2.5% experimental, 11.5% from theory, 12% total at nominal conditions, 15% shortly after start-up. With the accumulation of data and improved calculations there is hope to improve

[†]Calculations by M.Schmitt with the program PHOZPRMS [347].

Table 15.4: The PDF uncertainty on the cross section ratios (positive and negative asymmetric errors) as estimated using LHAPDF. Clearly normalising to the 250-500 GeV/c^2 mass bin is superior compared to a normalisation relative to the Z peak (70-120 GeV/c^2).

Mass [GeV/c^2]	R($\frac{M}{250-500}$) PDF + [%]	PDF - [%]	R($\frac{M}{Zpeak}$) PDF + [%]	PDF - [%]
500-600	+1.5	-1.5	+4.6	-4.2
1000+	+5.2	-4.8	+7.8	-7.1
2000+	+10.7	-7.8	+12.9	-9.4

this number by making progress in our understanding of PDF, electro-weak radiative corrections and K-functions.

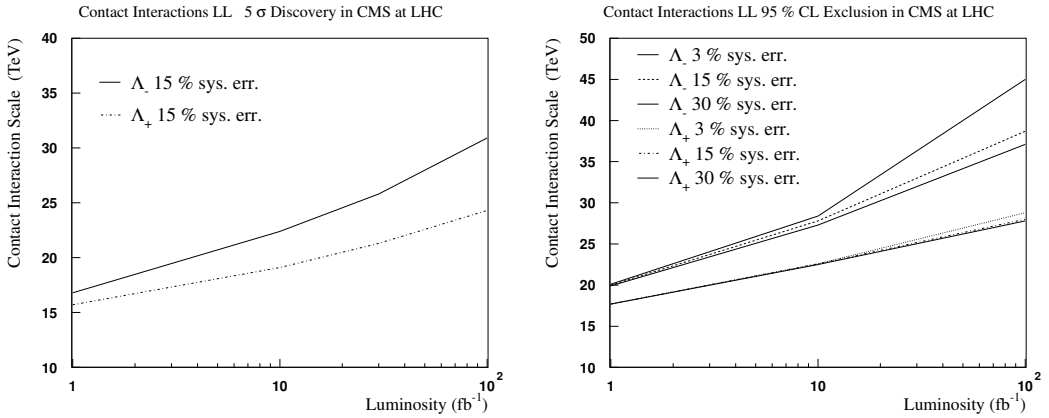

Figure 15.4: Five sigma discovery reach (left) and sensitivity at 95 % CL(right) for contact interactions in the dimuon channel for different luminosities and signs of the interference.

The discovery reach for a given model is determined by constructing a negative log-likelihood function combining the deviations between measurements and predictions, including the contact interaction contributions, for all simulated data points. The error on a deviation consists of three parts, which are combined in quadrature: a statistical error, an experimental systematic error and a theoretical uncertainty. The log-likelihood function is integrated in the physically allowed region (all positive Λ for positive interference and all negative Λ for negative interference) to derive the five standard deviations σ discovery reach and one-sided lower limits at 95% confidence level on the scale.

The discovery reach is summarised in Figure 15.4. The sensitivity is dominated by the cross section measurement, the contribution of the forward-backward asymmetry is minor. The sensitivity for negative interference is substantially better. Even at the highest luminosities the statistical errors at LHC play a major role, as evident from the comparison of the cases with total systematic uncertainties of 3, 15 and 30 %. This is not surprising as the Drell-Yan process is probing directly masses up to $\sim$ 4–5 TeV/c^2, where due to the steeply falling cross sections the statistical errors remain important for all considered luminosities.

15.3 Search for contact interactions with dijets

New physics at a scale Λ above the mass of the final state is effectively modelled as a contact interaction. Here the propagator for a particle of mass $M \sim \Lambda$ exchanged between quarks, or exchanged between constituent particles inside two interacting composite quarks, shrinks to a single point and gives a contact interaction. Quark contact interactions, for example those that arise from a left-handed interaction among composite quarks [122, 123], will always produce a rise in rate relative to QCD at high dijet mass or high inclusive jet E_T. However, observation in the mass distribution alone requires precise understanding of the QCD rate as a function of dijet mass, which is complicated by the large systematic uncertainties discussed in section 4.1.6. Angular distributions benefit from much smaller systematic uncertainties. The contact interaction is often more isotropic than the QCD background, since QCD is dominated by t-channel scattering and produces jets predominantly in the forward direction. Our analysis uses the dijet ratio, discussed in section 4.1.5, to measure the angular distribution as a function of dijet mass, and see any contact interactions which affect the dijet angular distribution [749].

15.3.0.1 Contact interaction sensitivity estimates

The QCD background distribution for the dijet ratio was discussed in section 14.5. In Figure 15.5 we show a smooth dijet ratio for QCD, estimated at 0.6 from the fit to the full simulation. The error bars shown in Figure 15.5 are the statistical uncertainties expected with $1\,\text{fb}^{-1}$ and the jet trigger prescales discussed in section E.4.3.2. The uncertainties are calcu-

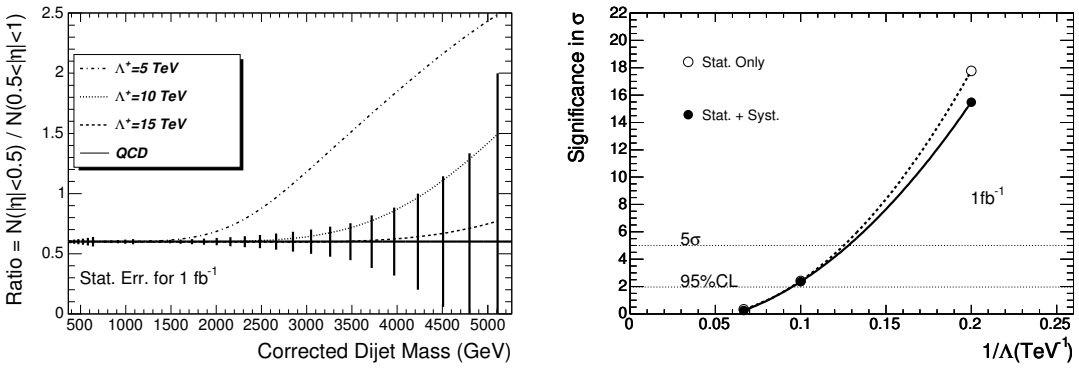

Figure 15.5: Left) The expected value and statistical error of the dijet ratio of QCD in the CMS detector for $1\,\text{fb}^{-1}$ (solid) is compared with QCD plus a quark contact interaction at a scale Λ^+ of 15 TeV (dashed), 10 TeV (dotted) and 5 TeV (dot-dashed). Right) The significance with statistical uncertainties only (open circles) and with all uncertainties (solid circles) of the difference between QCD alone and QCD plus a quark contact interaction is plotted vs $1/\Lambda^+$ and fit with a quadratic function. Horizontal lines show the 5σ and 95% CL levels.

lated using Poisson statistics at high dijet mass, where few events are expected and Gaussian statistics is less accurate. In Figure 4.7 we presented a lowest order calculation of both QCD and a contact interaction among left-handed quarks. The signal in Figure 15.5 is estimated by scaling the lowest order contact interaction calculation of Figure 4.7 by the ratio of our full simulation prediction for QCD to the lowest order QCD calculation: signal = contact $\times$ 0.6 / QCD. Systematic uncertainties on the dijet ratio are small, as discussed in section 4.1.6 and demonstrated in Figure 4.8. The calculated chisquared between QCD and the contact

interaction signal, including all uncertainties on the dijet ratio, is listed in Table 15.5. In Fig-

Table 15.5: Chisquared between signal and background. For each luminosity and contact interaction scale considered we list the chisquared between QCD alone and QCD plus a contact interaction, for the case where only statistical uncertainties are included (Stat), and for the case where both statistical and systematic uncertainties are included (All).

Luminosity	$100\,\text{pb}^{-1}$			$1\,\text{fb}^{-1}$			$10\,\text{fb}^{-1}$		
Λ^+(TeV)	5	10	15	5	10	15	5	10	15
χ^2 (Stat)	18.3	.090	.0037	316	5.82	.107	3652	133	4.15
χ^2 (All)	16.7	.082	.0011	240	5.55	.061	1340	124	3.56

ure 15.5 we show the significance in σ, estimated as $\sqrt{\chi^2}$, compared to a smooth fit as a function of $1/\Lambda^+$. The anticipated capability of CMS with $1\,\text{fb}^{-1}$ to exclude contact interactions at 95% CL or discover them at 5σ can be read off Figure 15.5, and they are listed in Table 15.6. This includes the uncertainty on Λ due to the anticipated 5% uncertainty on the observed jet energy. The same analysis is repeated for $100\,\text{pb}^{-1}$ and $10\,\text{fb}^{-1}$ and the results are also listed in Table 15.6. The systematic uncertainties on the dijet ratio reduced the CMS sensitivity to a contact interaction between 0.1 and $0.3\,\text{TeV/c}^2$ depending on luminosity and level of significance. To see how quickly CMS jet data will extend the search for new physics, we note that with $100\,\text{pb}^{-1}$ our anticipated 95% CL sensitivity, $\Lambda^+ < 6.3\,\text{TeV}$, is more than twice the sensitivity of the DØ search($\Lambda^+ < 2.7\,\text{TeV}$ at 95% CL)[121]. We note that our contact interaction sensitivity to composite quarks in Table 15.6 is roughly twice our mass resonance sensitivity to excited states of composite quarks in Table 14.5, and is equivalent to observing or excluding a quark radius of order 10^{-18} cm.

Table 15.6: Sensitivity to contact interactions with $100\,\text{pb}^{-1}$, $1\,\text{fb}^{-1}$, and $10\,\text{fb}^{-1}$. We list the largest value of the contact interaction scale we expect to be able to exclude at a confidence level of 95% or greater, and the largest value we expect to be able to discover with a significance of 5σ or greater. Estimates include both statistical and systematic uncertainties.

	95% CL Excluded Scale			5σ Discovered Scale		
Luminosity	$100\,\text{pb}^{-1}$	$1\,\text{fb}^{-1}$	$10\,\text{fb}^{-1}$	$100\,\text{pb}^{-1}$	$1\,\text{fb}^{-1}$	$10\,\text{fb}^{-1}$
Λ^+(TeV)	<6.2	<10.4	<14.8	<4.7	<7.8	<12.0

15.4 Heavy Majorana neutrinos and right-handed bosons

15.4.1 Introduction

This study is exploring the left-right (LR) symmetric model $SU_C(3)\otimes SU_L(2)\otimes SU_R(2)\otimes U(1)$ [724, 725, 750] at LHC. The model embeds the SM at the scale of the order of 1 TeV and naturally explains the parity violation in weak interactions as a result of the spontaneously broken parity. It necessarily incorporates three additional gauge bosons W_R and Z' and the heavy right-handed Majorana neutrino states N. The Ns can be the partners (N_l) of the light neutrino states ν_l ($l = e, \mu, \tau$) and can provide their non-zero masses through the see-saw mechanism [726]. Given the results from the atmospheric, solar and reactor neutrino experiments the LR model is very attractive. In the framework of the LR symmetric model, we have studied the production and the experimental signature of heavy Majorana neutrinos and the associated heavy gauge bosons. The detailed analysis is presented in [751].

Existing experimental data constrain the Z' mass to the values $O(1)$ TeV/c^2 [752]. The lower bound on the W' mass derived from the $K_L - K_S$ mass difference is quite stringent, $M_{W'} \gtrsim 1.6$ TeV [753], however with some uncertainties from the low energy QCD corrections to the kaon system. The direct searches for W' at the Tevatron yield bounds $M_{W'} \gtrsim 720$ GeV/c^2 assuming a light (keV-range) N, and $M_{W'} \gtrsim 650$ GeV/c^2 assuming $M_N < M_{W'}/2$ [754]. These bounds are less stringent in more general LR models.

15.4.2 Heavy Majorana neutrino production and decay

The cross sections of $pp \to W_R \to l + N_l + X$ (the process studied here), and $pp \to Z' \to N_l + N_l + X$ (where $N_l \to l + j_1 + j_2$) depend on the value of the coupling constant g_R, the parameters of the CKM mixing matrix for the right-handed sector, the $W_R - W_L$ and $Z' - Z$ mixing strengths, and the masses of the partners N_l of the light neutrino state. In the study presented here the mixing angles are assumed small, the right-handed CKM matrix is identical to the left-handed one and $g_R = g_L$. With these assumptions the Z' is about 1.7 times heavier than W_R and the production cross-section for $pp \to W_R \to eN_e$ is found to be at least one order of magnitude higher than for the $pp \to Z' \to N_eN_e$ process. Finally it is assumed that only the lightest M_{N_e} is reachable at the LHC. In the case of degenerated masses of N_l, the channels with μ's and τ's are open resulting in the increase of the cross section of the process studied here by a factor of ~ 1.2. The analysis is performed in the M_{W_R}, M_{N_e} parameter space. For the benchmark point considered (referred to as (LRRP)) $M_{N_e} = 500$ GeV/c^2 and $M_{W_R} = 2000$ GeV/c^2.

For the signal event generation and calculation of cross sections, the PYTHIA Monte Carlo program is used that includes the LR symmetric model with the standard assumptions mentioned above and CTEQ5L parton distribution functions. The fraction of $pp \to W_R^+$ ($pp \to W_R^-$) reactions as a function of M_{W_R} changes from $\simeq 70\%$($\simeq 30\%$) at $M_{W_R} \simeq 1$ TeV/c^2 to $\simeq 95\%$($\simeq 5\%$) at $M_{W_R} \simeq 10$ TeV/c^2. For W_R boson masses higher than $M_{W_R} \simeq 2$ TeV/c^2 the production of W_R^+ boson dominates. The W_R mass region above 1 TeV/c^2 is studied since smaller masses are excluded by indirect analyses [755].

The signal and background data sample are simulated using the GEANT based CMS full detector simulation [8] and reconstruction package [10].

15.4.3 Analysis

The two major backgrounds considered in this study are the Z+jets and $t\bar{t}$ production. In the event selection two isolated electrons and at least two jets are required. The dielectron invariant mass M_{ee} is required to be above 200 GeV/c^2 to suppress the Z+jets Standard Model background. The invariant mass of each electron with the two leading jets M_{ejj} ($M_{N_e}^{\text{cand}}$ is formed. The M_{eejj}, (W_R boson candidate) invariant mass is required to be above 1 TeV/c^2. After this requirement the Standard Model background is suppressed as shown in Figure 15.6.

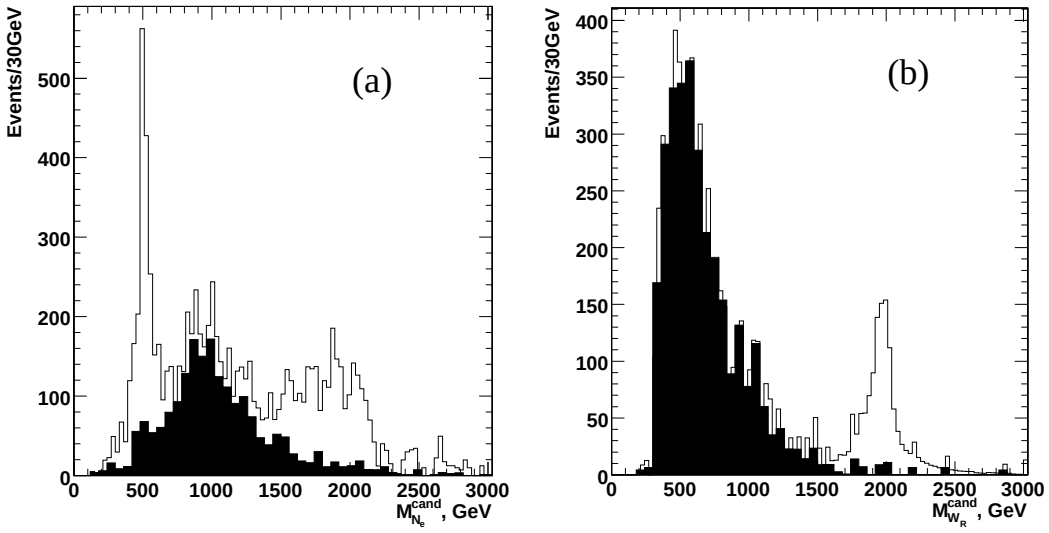

Figure 15.6: M_{ejj} for the signal overlaid with the SM background (shaded histogram) for 30 fb^{-1}: (a) M_{eejj} >1 TeV/c^2, (b) M_{eejj} <1 TeV/c^2.

The total W_R mass the reconstruction efficiency for $M_{W_R} = 2$ TeV/c^2 and for neutrino masses above 500 GeV/c^2 is between 20% and 25% while for neutrino masses much smaller than the W_R mass the reconstruction efficiency drops due to the significant overlap of the heavy neutrino decay products in $\eta - \phi$.

15.4.4 Results

The 5 sigma discovery contour in the $(M_{W_R}; M_{N_e})$ plane is shown in Figure 15.7 for 1 and 30 fb^{-1}. With 30 fb^{-1} a 5 sigma observation of W_R and N_e with masses up to 4 TeV/c^2 and 2.4 TeV/c^2 respectively can be achieved. The signal at the LRRP test point (W_R of 2 TeV/c^2 and N_e 500 GeV/c^2) is observable already after one month of running at low luminosity.

15.5 Little Higgs models

15.5.1 Introduction

The Little Higgs model [656] provides an alternative mechanism of electroweak symmetry breaking keeping a light Higgs boson free from one-loop divergences of SM. It breaks a global symmetry spontaneously and invokes a number of new particles of masses in TeV scale. A heavy singlet quark of charge 2/3, marked as T, is the lightest among them and hence we study the viability of its observation with limited integrated luminosity.

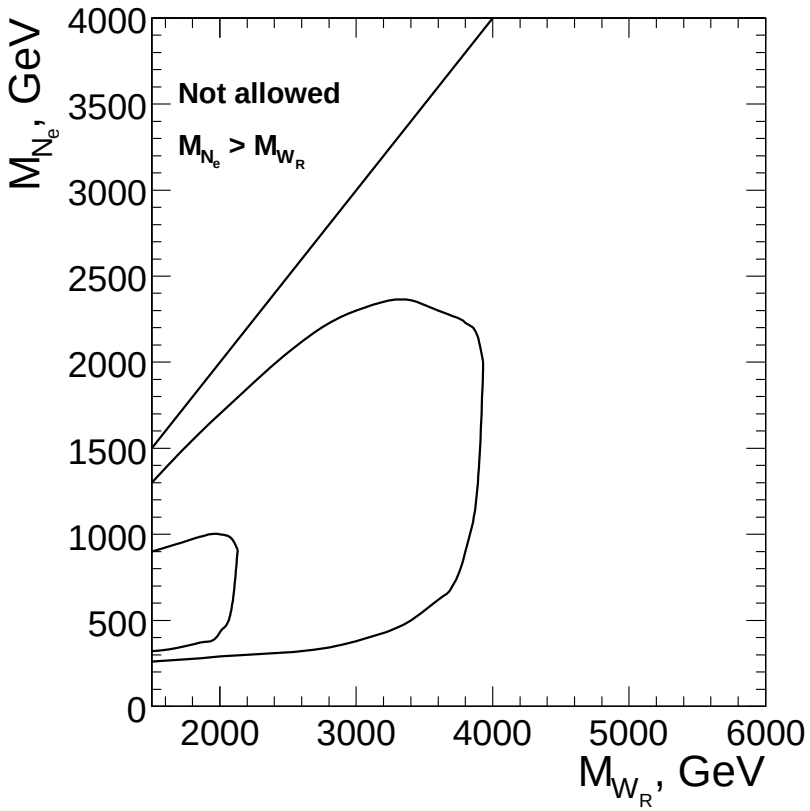

Figure 15.7: CMS discovery potential of the W_R boson and right-handed Majorana neutrinos of the Left-Right Symmetric model for the integrated luminosity $L_t = 30\,\text{fb}^{-1}$ (outer contour) and for $L_t = 1\,\text{fb}^{-1}$ (inner contour)

The heavy quark T acquires its mass via Yukawa interactions of two gauge groups with couplings λ_1 and λ_2 which are of similar order. T has three dominant decay modes, the corresponding branching ratios following the relation: $BR(T \rightarrow t\ h) = BR(T \rightarrow tZ) = \frac{1}{2}BR(T \rightarrow bW)$.

15.5.2 Analysis

The decay channel $\mathrm{T} \rightarrow \mathrm{tZ}$, with leptonic decays of Z and W bosons, provides a clean signature at the LHC environment. This channel has not been previously studied in CMS and the work presented here is a feasibility study. Further details can be found in [756].

The signal samples were generated with PYTHIA 6.227 [24] and the T production was mimicked by activating the fourth quark generation through the W-b fusion. The T quark mass was set to 1 TeV/c^2 and was treated as a narrow resonance. The CMS full detector simulation was performed with OSCAR [8] and ORCA [10] while pile-up events corresponding to the low luminosity running period of the LHC were taken into account. The major backgrounds considered in this analysis were: $t\bar{t}$, ZW+jets, ZZ+jets, WW+jets, $\mathrm{Zb\bar{b}}$, and Z+jets.

The main selection requirements are summarised below:

- Events are required to pass the "double electron" or "double muon" L1 and HLT trigger criteria.
- Electrons are required to have p_T >20 GeV/c and muons $p_T > 10$ GeV/c

- The combined transverse momentum of the same flavour opposite sign lepton pair is required to be $p_T^{\ell\ell} > 100$ GeV/c. The invariant mass of the pair is required to be consistent with the nominal Z mass within 10 GeV/c.
- A further third lepton is required in the event ($e^{\pm}$ with p_T >20 GeV/c or $\mu^{\pm}$ with p_T >15 GeV/c); The combined transverse momentum of the third lepton with the missing transverse energy is required to be greater than 60 GeV/c. In addition the transverse mass of the third lepton with the missing transverse energy is required to be less than 120 GeV/c^2, to be consistent with the W boson transverse mass.
- Exactly one jet compatible with a b-jet and with calibrated transverse momentum more than 30 GeV/c is required.
- The combined transverse momentum of the W boson and the b-jet should be more than 150 GeV/c, while their invariant mass is required to be in the range $(110-220)$ GeV/c^2.
- The combined $Z\ W\ b$ system invariant mass is required to be in the mass range of the search for heavy quark, namely $(850 - 1150)$ GeV/c^2.

The SM background ZZ $\rightarrow$ leptonic, is the only background that gives non-zero contribution (still less than 1 event at luminosity 30 fb^{-1}). The total efficiency for the signal selection is $(9.7 \pm 0.4)\%$. Assuming the production cross section of T $\rightarrow$ t Z to be 192 fb for M_T = 1 TeV/c^2 (for the case of $\lambda_1 = \lambda_2$) and folding in the branching ratios involved, a total of $N_S = 2.1 \pm 0.1$ signal events are expected for 30 fb^{-1}. This implies that the discovery potential of the channel is rather limited.

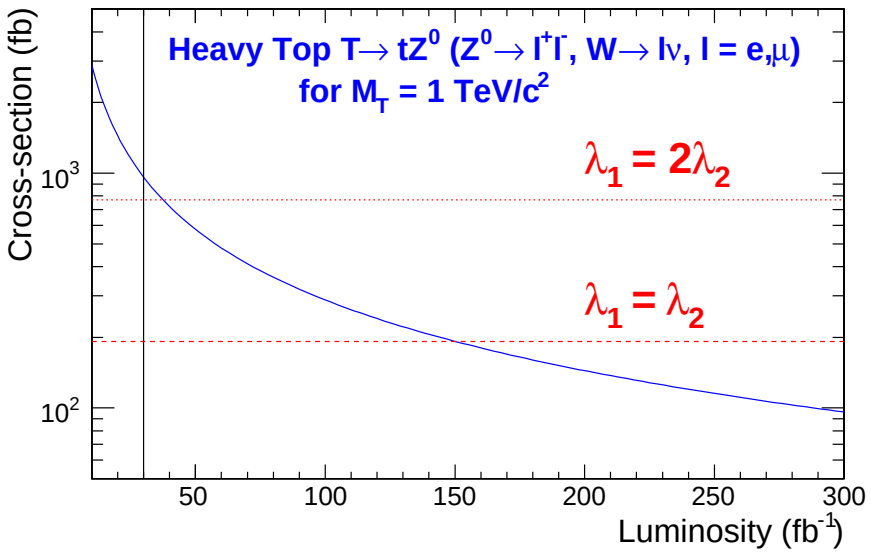

Figure 15.8: Minimum cross section required for a 5σ discovery for a heavy quark of mass M_T = 1 TeV/c^2 as a function of the luminosity. The horizontal lines correspond to the cross section values for the two cases of λ_1/λ_2. The vertical line indicates the luminosity of 30 fb^{-1} used for this analysis.

The statistical significance of the channel (S_{c12}, defined in Appendix A.1) is 2.5 with a signal-to-background ratio of 41 for 30 fb^{-1}. Taking into account systematic uncertainties from the electron energy scale, jet and missing energy scale and b-tagging efficiency uncertainty, the significance drops down to 2.0. Fig. 15.8 shows the signal cross section as a function of the integrated luminosity at the LHC, for establishing at 5σ level, single production of a heavy

quark of mass = 1 TeV/c^2. The luminosity needed for 5σ evidence is estimated to be around 150 fb^{-1} (40 fb^{-1}) for choices of parameters $\lambda_1 = \lambda_2$ ($\lambda_1 = 2\lambda_2$). The vertical line corresponds to the luminosity used for this analysis and demonstrates the inadequacy of statistics for a luminosity of 30 fb^{-1}.

15.6 Same sign top

At the LHC dileptonic $t\bar{t}(+jets)$ events can be selected with a relatively high signal-to-noise ratio and efficiency. Within the clean sample of such events, both leptons (electrons and muons) have an opposite electric charge. In several models beyond the Standard Model however, $tt/\overline{tt}(+jets)$ topologies are predicted where both leptons have an equal electric charge. The signal excess is highly enhanced by the application of a combined likelihood variable described in [283]. The likelihood variable is designed to differentiate the lepton from the W boson decay from leptons arising for example in QCD jets or from fake reconstructions. The signal of new physics can be diluted by the mis-identification of the electric charge of the leptons in Standard Model $t\bar{t}(+jets)$ events and the mis-identification of the leptons from the W decay themselves. The observability of an excess of same-sign signals above the mis-reconstruction of the Standard Model background is determined. The details of the analysis are mentioned in [757].

The jets in the final state are reconstructed with an Iterative Cone jet clustering algorithm using a cone size of ΔR = 0.5. Input objects for the cones are selected from all calorimeter towers above a pseudo-rapidity dependent energy threshold determined from the average underlying event energy deposits [164]. The energy scale of the reconstructed jets is calibrated with corrections from Monte Carlo studies. The primary vertices in the proton bunch crossing are determined, and the vertex with the highest transverse momentum is taken as the one of the hard scattering. Via a track-based algorithm, jets are rejected if they do not match with this hard primary vertex.

The leptons are reconstructed and identified using the methods described in [283]. A likelihood variable is used to suppress leptons from the heavy flavour quark background exploiting several reconstruction aspects of leptons in the CMS detector. This likelihood is determined for each muon or electron in the final state in order to enhance the purity of choosing the correct lepton from the leptonic W decay. The combined likelihood includes observables as tracker isolation, calorimeter isolation, vertex matching significance, transverse momentum of the lepton and angular distance to the closest jet. For the electron likelihood a variable reflecting the reconstruction quality is added. The two muons or electrons having the largest combined likelihood ratio value are taken as the hard leptons of interest.

The inclusive single-muon, single-electron, double muon and double electron triggers are applied as described in [506]. The event should be triggered in at least one of these streams. In total 88.4% , 77.4% and 79.2% of respectively the $\mu\mu$, the ee and the μe signal events remain after applying the trigger criteria. The event is required to have at least 2 jets with a calibrated E_T above 25 GeV. These jets need to have a pseudo-rapidity in the range $|\eta| < 2.4$ and a b-tag discriminant larger than 0.5 [156]. The reconstructed hard leptons are required to have transverse momentum p_T exceeding 25 GeV/c in the pseudo-rapidity range of $|\eta| < 2.4$ and a combined likelihood variable larger than 0.05.

In Table 15.7 the efficiencies and signal-to-noise ratios are shown after each selection step. Applying all cuts a signal-to-noise ratio of 4.7, 3.1 and 8.3 is obtained for respectively the

Table 15.7: Overview of the selection criteria applied on the events using simulated events with pile-up collisions included. The expected number of events are rescaled to a dataset of 1 fb^{-1} taking into account the respective Leading-Order cross-sections of the processes.

	$\mu\mu$	μe and ee	$t\bar{t} \to \tau + X$	Other $t\bar{t}$	$W^{\pm}W^{\mp}$	$Z + jets$	S/N
Before selection	6915.0	20745.0	34606.2	485973.2	189951.7	578033.3	0.0078
Trigger	6114.7	16314.8	17415.6	100137.2	41288.4	266366.7	0.017
Two jets E_T >25 GeV	4398.2	11982.7	13560.9	93858.2	20593.8	66146.7	0.032
b-tag criteria	989.8	2485.4	2289.6	8784.7	133.5	240.0	0.13
Two leptons identified	888.2	30.1	375.8	801.6	1.7	73.3	1.30
Two leptons selected	481.5	0.07	48.4	3.01	0.4	53.3	4.7
Efficiency (in %)	6.96	0.0003	0.14	0.0006	0.00022	0.0092	
Opposite-sign	481.3	0	48.3	2.19	0	53.3	
Same-sign	0.2	0.07	0.1	0.82	0.4	0	
	ee	μe and $\mu\mu$	$t\bar{t} \to \tau + X$	Other $t\bar{t}$	$W^{\pm}W^{\mp}$	$Z + jets$	S/N
Before selection	6915.0	20745.0	34606.2	485973.2	189951.7	578033.3	0.0078
Trigger	5354.8	17074.7	17415.6	100137.2	41288.4	266366.7	0.015
Two jets E_T >25 GeV	3960.9	12420.0	13560.9	93858.2	20593.8	66146.7	0.029
b-tag criteria	802.7	2672.4	2289.6	8784.7	133.5	240.0	0.11
Two leptons identified	724.5	34.6	453.8	2283.6	73.1	126.7	0.57
Two leptons selected	285.0	0.3	37.5	5.2	0.8	53.3	3.1
Efficiency (in %)	4.12	0.0013	0.11	0.0011	0.00044	0.0092	
Opposite-sign	279.6	0.3	36.8	4.1	0.4	46.7	
Same-sign	5.4	0	0.7	1.1	0.4	6.7	
	$e\mu$	$\mu\mu$ and ee	$t\bar{t} \to \tau + X$	Other $t\bar{t}$	$W^{\pm}W^{\mp}$	$Z + jets$	S/N
Before selection	13830.0	13830.0	34606.2	485973.2	189951.73	578033.3	0.016
Trigger	10960.0	11469.5	17415.6	100137.2	41288.4	266366.7	0.030
Two jets E_T >25 GeV	8021.8	8359.1	13560.9	93858.2	20593.8	66146.7	0.061
b-tag criteria	1682.7	1792.5	2289.6	8784.7	133.5	240.0	0.25
Two leptons identified	1500.6	66.4	822.1	3001.6	30.2	20.0	0.88
Two leptons selected	722.7	0.9	85.2	6.3	0.4	0	8.3
Efficiency (in %)	5.23	0.0065	0.25	0.0013	0.00022	0	
Opposite-sign	715.5	0.9	83.8	4.9	0	0	
Same-sign	7.2	0	1.3	1.4	0.4	0	

$\mu\mu$, the ee and the $e\mu$ final state. Cross-talk between these three considered final states is by construction not possible. As the amount of selected WW and $Z + jets$ events in Table 15.7 is small, their contribution is alternatively estimated by multiplying the efficiencies of the event selection without the b-tagging and the individual b-tagging selection cut efficiency under the assumption that both selection cuts are uncorrelated.

It is illustrated [757] that from the selected topology of dilepton $t\bar{t}$ events, a ratio $R = \frac{N_{++,--}}{N_{+-}}$ can be determined which is sensitive to physics beyond the Standard Model. In the ratio the total amount of events with equally charged leptons is divided by the total amount of events with opposite charged leptons. As the efficiency of reconstructing the leptons electric charge is very high, we can neglect the amount of selected $pp \to tt$ or $pp \to \overline{tt}$ events observed with two opposite-charged leptons. Using the uncertainty on the ratio R, the significance of the observation of new physics channels $pp \to tt$ or $pp \to \overline{tt}$ is determined as a function of the cross section (see Figure 15.9). The dimuon channel has a larger sensitivity compared to the decay channels with electrons. This is caused by the electron reconstruction where a large fraction of electron energy clusters are matched with a wrong track resulting in a charge ambiguity.

It is assumed that the new physics processes beyond the Standard Model have a similar kinematic topology compared to the $t\bar{t}$ process, therefore the selection efficiency of the new physics channels is taken equal to that of the Standard Model $t\bar{t}$ process. Several models predict an excess of events with same-sign leptons in this topology, via the process $pp \to tt/\overline{tt}$ or $pp \to tt/\overline{tt} + b/c$. These models are motivated by Flavour Changing Neutral Currents (FCNC) [758, 759], topcolour-assisted Technicolour (TC2) [760] or supersymmetry [761]. With a measurement of R these kinematically similar processes $pp \to tt/\overline{tt}$ can be observed with 30 fb^{-1} of integrated luminosity if they have a cross section above 1 pb. Because a ratio of kinematically similar event topologies is measured, most of the experimental and theoretical systematic uncertainties cancel. The uncertainty of the background cross sections on the significances shown in Figure 15.9 is found to be negligible. A feasibility study is performed to estimate the potential uncertainty on the mis-identification efficiency of the electric charge of electrons and muons from Z boson decays [757]. The effect on the significance of the excess of $tt/\overline{tt}$ events is found to be negligible.

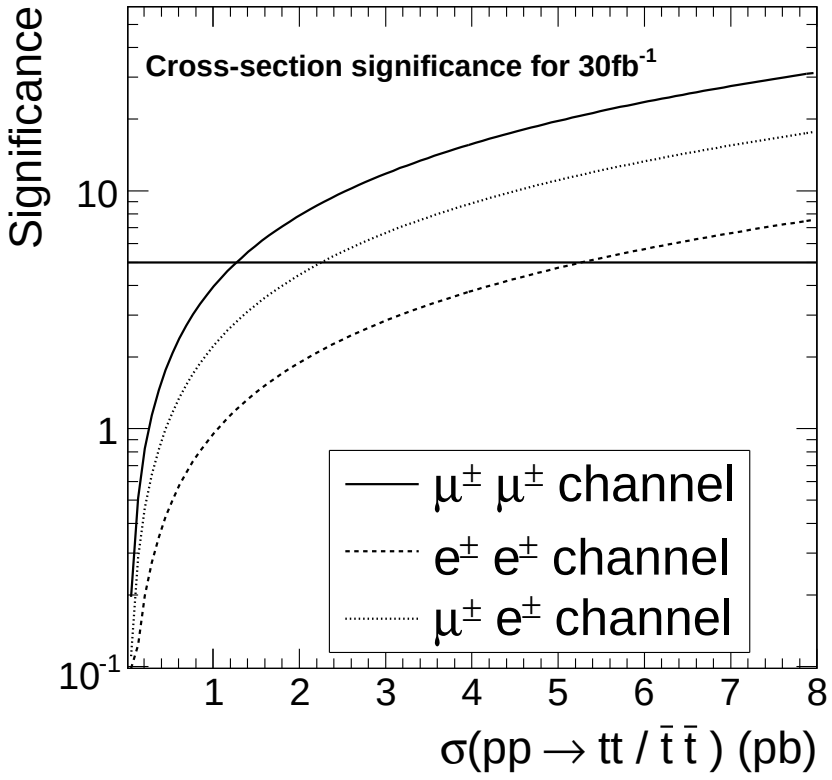

Figure 15.9: For an integrated luminosity of 30 fb^{-1} the significance of the same-sign tt or $\overline{tt}$ excess above the Standard Model events is indicated as a function of the cross-section of the inclusive process $pp \to tt/\overline{tt}$.